MULTI-VIEW INDOOR SCENE RECONSTRUCTION FROM COMPRESSED THROUGH-WALL RADAR MEASUREMENTS USING A JOINT BAYESIAN SPARSE REPRESENTATION

V. H. Tang, A. Bouzerdoum, S. L. Phung, and F. H. C. Tivive

School of Electrical, Computer and Telecommunications Engineering,
University of Wollongong, NSW, 2522, Australia

ABSTRACT

This paper addresses the problem of scene reconstruction, incorporating wall-clutter mitigation, for compressed multi-view through-the-wall radar imaging. We consider the problem where the scene is sensed using different reduced sets of frequencies at different antennas. A joint Bayesian sparse recovery framework is first employed to estimate the antenna signal coefficients simultaneously, by exploiting the sparsity and correlations between antenna signals. Following joint signal coefficient estimation, a subspace projection technique is applied to segregate the target coefficients from the wall contributions. Furthermore, a multitask linear model is developed to relate the target coefficients to the scene, and a composite scene image is reconstructed by a joint Bayesian sparse framework, taking into account the inter-view dependencies. Experimental results show that the proposed approach improves reconstruction accuracy and produces a composite scene image in which the targets are enhanced and the background clutter is attenuated.

***Index Terms*—** Multi-view through-the-wall radar imaging, wall clutter mitigation, compressed sensing, joint Bayesian sparse recovery.

1. INTRODUCTION

Through-the-wall radar imaging (TWRI) is emerging as a powerful technology for numerous civilian and military applications [1,2]. In practice, TWRI faces several interferences, such as layover and shadow effects, which impede target detection and localization. For example, when the antenna is placed facing a strong reflective target with another weak target behind, layover effects occur, rendering the detection of the weak target more difficult, or impossible. Further, the target reflectivity depends highly on the sensing aspect angle. Target reflections may be strong if sensed from the front wall, but may be weak when illuminated from the side wall, and vice versa. These problems can be addressed by using multi-view or multi-location sensing and then combining the data acquired from different vantage points to enhance image formation and target detection.

Multi-view TWRI methods typically involve image formation at individual views, followed by image fusion [2, 3], target image correction [4], or target detection [5]. These existing methods, however, are not concerned with the TWRI problem in the compressed sensing (CS) context [6, 7]. The full data volume at each view is required to form the images. In the past decade, CS has been used for TWRI to save data acquisition, reduce computation cost, and improve image formation and fusion [8–11]. More recently, CS-based techniques have been proposed which combine wall-clutter mitigation with image formation [12–14]. These methods, however, are suitable for single-view TWRI problem only; they do not consider the inter-view correlations in the imaging model.

In this paper, we propose a new approach for unifying wall-clutter mitigation and compressed multi-view TWRI scene reconstruction. First, a joint Bayesian sparse model is employed to reconstruct the antenna signal coefficients simultaneously, by exploiting both the sparsity and correlations between antenna signals. This joint model differs from the single-signal CS recovery model presented in [12, 14], where each antenna signal is recovered independently. This paper demonstrates that the proposed joint Bayesian CS model requires far fewer measurements and yields higher recovery accuracy than the single-signal CS model. Furthermore, a subspace projection technique is applied directly to the estimated signal coefficients to segregate the wall reflections from target returns. For scene reconstruction, a multitask linear model is developed to relate the clutter-free signal coefficients to the image of the scene. A composite image of the scene is finally recovered using joint sparse Bayesian learning.

The remainder of the paper is organized as follows. Section 2 introduces the multi-view TWRI signal model. Section 3 describes the proposed approach, including joint Bayesian antenna signal coefficient estimation, wall-clutter mitigation, and joint Bayesian image reconstruction. Section 4 presents experimental results and analysis. Section 5 gives concluding remarks.

2. MULTI-VIEW TWRI SIGNAL MODEL

Consider a monostatic multi-view TWRI system illuminating a scene behind a wall or inside an enclosed structure. Assume that the scene containing P targets is imaged at L locations or views, by shifting the same antenna array to new locations vertically or horizontally along the front and side walls. At each view, the TWRI system uses M antenna locations and N narrowband signals to scan the scene. Let $z_l(m,n)$ denote the signal of frequency f_n, received by the m-th antenna from the l-th view. This signal can be expressed as

$$z_l(m,n) = \sigma_w e^{-j2\pi f_n \tau_{m,w}} + \sum_{p=1}^{P} \sigma_p e^{-j2\pi f_n \tau_{m,p}} + \nu_l(m,n), \tag{1}$$

where σ_w is the reflectivity of the wall, σ_p is the reflectivity of the p-th target, $\tau_{m,w}$ is the round-trip travel time of the signal from the m-th antenna to the wall, $\tau_{m,p}$ is the round-trip travel time of the

This work was partially supported by a grant from the Australian Research Council.

signal from the m-th antenna to the p-th target, and $\nu_l(m,n)$ is the noise term.

Assume that the scene is partitioned into a rectangular grid consisting of Q pixels. Let $s_l(q)$ denote a weighted indicator function defined as

$$s_l(q) = \begin{cases} \sigma_w, & \text{if the wall occupies the } q\text{-th pixel;} \\ \sigma_p, & \text{if the } p\text{-th target occupies the } q\text{-th pixel;} \\ 0, & \text{otherwise.} \end{cases} \quad (2)$$

We denote by $\mathbf{z}_{l,m}$ and $\boldsymbol{\nu}_{l,m}$ the column vectors containing, respectively, the frequency measurements and the noise samples received by the m-th antenna at the l-th view, see Eq. (1). Similarly, let $\mathbf{s}_l$ be the lexicographically ordered column vector containing the pixel values of the l-th view. It follows from Eqs. (1) and (2) that

$$\mathbf{z}_{l,m} = \boldsymbol{\Psi}^{l,m}\, \mathbf{s}_l + \boldsymbol{\nu}_{l,m}, \quad (3)$$

where $\boldsymbol{\Psi}^{l,m}$ is an $N \times Q$ matrix whose nq-th element $\Psi^{l,m}_{nq} = e^{-j2\pi f_n \tau_{m,q}}$, with $\tau_{m,q}$ being the propagation delay between the m-th antenna and the q-th pixel. By concatenating the received signals at all M antennas, we can write

$$\mathbf{z}_l = \boldsymbol{\Psi}_l\, \mathbf{s}_l + \boldsymbol{\nu}_l, \quad (4)$$

where $\mathbf{z}_l = [\mathbf{z}_{l,0}^T, \ldots, \mathbf{z}_{l,M-1}^T]^T$, $\boldsymbol{\Psi}_l = [{\boldsymbol{\Psi}^{l,0}}^T, \ldots, {\boldsymbol{\Psi}^{l,M-1}}^T]^T$, and $\boldsymbol{\nu}_l = [{\boldsymbol{\nu}_{l,0}}^T, \ldots, {\boldsymbol{\nu}_{l,M-1}}^T]^T$.

The image of the scene $\mathbf{s}_l$ can be recovered from (4) by applying delay-and-sum (DS) beamforming or backprojection [1]. However, this approach is suitable for single-view TWRI only where the image at each view is reconstructed independently, ignoring the inter-view correlations. Note that before image formation, the wall contributions need to be removed or significantly reduced. In the next section, we present a new approach for compressed multi-view TWRI which incorporates wall clutter mitigation and takes into account the correlations between antenna signals and inter-view dependencies.

3. JOINT BAYESIAN MULTI-VIEW TWRI MODEL

This section presents the proposed approach for compressed multi-view TWRI. First, the antenna signals are represented by a sparsifying dictionary. Then, the signal coefficients are simultaneously estimated using a joint Bayesian sparse framework. A subspace projection technique is applied to the estimated coefficients to segregate the wall returns from the target coefficients. Finally, a multitask linear model is developed which combines the single view scenes with a composite scene. All the scenes are recovered jointly using a Bayesian approach.

3.1. Joint Signal Coefficient Estimation

The received signal $\mathbf{z}_{l,m}$ can be sparsely represented using a dictionary $\mathbf{W} \in \mathbb{R}^{N \times R}$ containing R ($R \geq N$) basis functions or atoms,

$$\mathbf{z}_{l,m} = \mathbf{W}\, \boldsymbol{\theta}_{l,m} + \boldsymbol{\epsilon}_{l,m}, \quad (5)$$

where $\boldsymbol{\theta}_{l,m}$ is a vector of signal coefficients and $\boldsymbol{\epsilon}_{l,m}$ is an error vector. In compressed multi-view TWRI, the reduced measurements $\mathbf{y}_{l,m}$ collected at the m-th antenna can be modeled as

$$\mathbf{y}_{l,m} = \boldsymbol{\Phi}_{l,m}\, \mathbf{z}_{l,m} = \mathbf{D}_{l,m}\, \boldsymbol{\theta}_{l,m} + \widetilde{\boldsymbol{\epsilon}}_{l,m}, \quad (6)$$

where $\boldsymbol{\Phi}_{l,m}$ is a $K \times N$ selection matrix ($K \ll N$) containing a single unit value in each row and each column, $\mathbf{D}_{l,m} = \boldsymbol{\Phi}_{l,m}\, \mathbf{W}$, and $\widetilde{\boldsymbol{\epsilon}}_{l,m} = \boldsymbol{\Phi}_{l,m}\, \boldsymbol{\epsilon}_{l,m}$.

Given the measurement vectors $\mathbf{y}_{l,m}$ and the dictionaries $\mathbf{D}_{l,m}$, the coefficient vectors $\boldsymbol{\theta}_{l,m}$ can be recovered using different approaches. In [9, 12], the vector $\boldsymbol{\theta}_{l,m}$ is recovered independently at each antenna. These methods, however, do not consider the correlations between antenna signals. In contrast, here we consider the multitask problem (6) as a joint sparsity model, which assumes the coefficient vectors $\boldsymbol{\theta}_{l,m}$ have overlapping support. The Bayesian sparse recovery framework is employed for jointly estimating the coefficient vectors $\boldsymbol{\theta}_{l,m}$ since it is more suitable for the TWRI problem than other simultaneous recovery algorithms [13].

Assuming that the noise term in (6) is zero-mean Gaussian with independent and identically distributed (i.i.d) components, the probability density function (pdf) of $\widetilde{\boldsymbol{\epsilon}}_{l,m}$ is given by

$$p(\widetilde{\boldsymbol{\epsilon}}_{l,m}) = \prod_{k=1}^{K} \mathcal{N}(\widetilde{\epsilon}_{l,m}(k) | 0, \beta^{-1}), \quad (7)$$

where β is the noise precision (variance = $1/\beta$). Therefore, the likelihood of $\boldsymbol{\theta}_{l,m}$ is a multivariate Gaussian function,

$$p(\mathbf{y}_{l,m} | \boldsymbol{\theta}_{l,m}, \beta) = (2\pi/\beta)^{-K/2} e^{-\frac{\beta}{2}||\mathbf{y}_{l,m} - \mathbf{D}_{l,m}\boldsymbol{\theta}_{l,m}||^2}. \quad (8)$$

The joint sparsity of the coefficient vectors is enforced using a shared prior imposed on $\boldsymbol{\theta}_{l,m}$ [15],

$$p(\boldsymbol{\theta}_{l,m} | \boldsymbol{\alpha}) = \prod_{i=1}^{R} \mathcal{N}(\theta_{l,m}(i) | 0, \alpha_i^{-1}). \quad (9)$$

Given the hyper-parameter vector $\boldsymbol{\alpha} = [\alpha_1, \ldots, \alpha_R]$, the posterior of $\boldsymbol{\theta}_{l,m}$ is a multivariate Student-t distribution with mean and covariance given by

$$\boldsymbol{\mu}_{l,m} = \Sigma_{l,m}\, \mathbf{D}_{l,m}^T\, \mathbf{y}_{l,m}, \quad (10)$$

$$\Sigma_{l,m} = (\mathbf{D}_{l,m}^T\, \mathbf{D}_{l,m} + \mathbf{A})^{-1}, \quad (11)$$

where $\mathbf{A} = \mathrm{diag}(\boldsymbol{\alpha})$. The problem now becomes searching for the hyper-parameter vector $\boldsymbol{\alpha}$, which can obtain by maximizing the logarithm of the marginal likelihood $\mathcal{L}(\boldsymbol{\alpha})$,

$$\widehat{\boldsymbol{\alpha}} = \arg\max_{\boldsymbol{\alpha}} \mathcal{L}(\boldsymbol{\alpha}) = \arg\max_{\boldsymbol{\alpha}} \sum_{m=0}^{M-1} \log p(\mathbf{y}_{l,m} | \boldsymbol{\alpha}). \quad (12)$$

The optimization problem in (12) is solved using a fast marginal likelihood maximization method [15–17]. Once the hyper-parameter vector $\widehat{\boldsymbol{\alpha}}$ has been obtained, the coefficient vector $\boldsymbol{\theta}_{l,m}$ is estimated by the mean of the posterior given by

$$\widehat{\boldsymbol{\theta}}_{l,m} = \boldsymbol{\mu}_{l,m}|_{\boldsymbol{\alpha}=\widehat{\boldsymbol{\alpha}}} = (\Sigma_{l,m}\, \mathbf{D}_{l,m}^T\, \mathbf{y}_{l,m})|_{\boldsymbol{\alpha}=\widehat{\boldsymbol{\alpha}}}. \quad (13)$$

The reconstructed vector $\widehat{\boldsymbol{\theta}}_{l,m}$ contains coefficients associated with wall returns that usually dominate the target signal. Therefore, before image reconstruction, we need to suppress or remove the coefficients related to the wall returns.

3.2. Wall Coefficient Mitigation

Usually, wall-clutter mitigation techniques are applied to the radar signals [18–21], which can be estimated from the recovered coefficients $\widehat{\boldsymbol{\theta}}_{l,m}$ as $\widehat{\mathbf{z}}_{l,m} \approx \mathbf{W}\, \widehat{\boldsymbol{\theta}}_{l,m}$, see Eq. (5). Here, however, we apply a subspace projection method directly to the estimated coefficients to segregate the wall contributions from the target returns.

Let $\widehat{\boldsymbol{\Theta}}$ denote a matrix comprising in its columns the antenna coefficients $\widehat{\boldsymbol{\theta}}_{l,m}$ obtained from all views. Using singular value decomposition, the matrix $\widehat{\boldsymbol{\Theta}}$ can be expressed as $\widehat{\boldsymbol{\Theta}} = \mathbf{U}\,\Sigma\,\mathbf{V}^H$, where $\mathbf{U} = [\mathbf{u}_1, \ldots, \mathbf{u}_R]$ and $\mathbf{V} = [\mathbf{v}_1, \ldots, \mathbf{v}_{ML}]$ are unitary matrices containing the left and right singular vectors, respectively; Σ is a matrix containing the singular values arranged in descending order along the main diagonal.

In TWRI, the wall returns are relatively stronger than the target reflections. Hence, the wall contributions are captured by the first few singular vectors associated with the dominant singular values. The wall subspace can be defined as

$$\mathbf{P}_{\mathrm{w}} = \sum_{i \in \mathcal{W}} \mathbf{u}_i\, \mathbf{v}_i^H, \tag{14}$$

where $\mathcal{W}$ denotes the index set of the singular vectors spanning the wall subspace [20]. To suppress the wall coefficients, the matrix $\widehat{\boldsymbol{\Theta}}$ is projected onto a subspace orthogonal to the wall subspace: $\widetilde{\boldsymbol{\Theta}} = (\mathbf{I} - \mathbf{P}_{\mathrm{w}}\mathbf{P}_{\mathrm{w}}^H)\,\widehat{\boldsymbol{\Theta}}$, where $\mathbf{I}$ denotes the identity matrix. Now the wall-clutter free coefficients $\widetilde{\boldsymbol{\Theta}}$ can be used for image reconstruction.

3.3. Joint Bayesian Sparse Scene Reconstruction

The scene can be formed by first reconstructing the radar signal from the target coefficients $\widetilde{\boldsymbol{\theta}}_{l,m}$, see Eq. (5), and then applying DS beamforming [9], or ℓ_1 minimization [12, 14]. However, these methods are designed for single-view image formation, which ignore the inter-view dependencies. Here, we formulate a multitask linear model that maps the clutter-free coefficients to the corresponding images of the scene and incorporates a composite coefficient vector representing the fused image of the scene. Using (3) and (5), we can relate the target coefficients to the scene as

$$\widetilde{\boldsymbol{\theta}}_{l,m} = \mathbf{W}^{-1}(\boldsymbol{\Psi}_{l,m}\,\widetilde{\mathbf{s}}_l + \boldsymbol{\nu}_{l,m} - \boldsymbol{\epsilon}_{l,m}) = \widetilde{\boldsymbol{\Psi}}_{l,m}\,\widetilde{\mathbf{s}}_l + \widetilde{\boldsymbol{\eta}}_{l,m}, \tag{15}$$

where $\widetilde{\mathbf{s}}_l$ is the l-th view target scene, $\widetilde{\boldsymbol{\Psi}}_{l,m} = \mathbf{W}^{-1}\,\boldsymbol{\Psi}_{l,m}$, and $\widetilde{\boldsymbol{\eta}}_{l,m} = \mathbf{W}^{-1}(\boldsymbol{\nu}_{l,m} - \boldsymbol{\epsilon}_{l,m})$. By stacking the coefficients belonging to the l-th view, we can rewrite

$$\widetilde{\boldsymbol{\theta}}_l = \widetilde{\boldsymbol{\Psi}}_l\,\widetilde{\mathbf{s}}_l + \widetilde{\boldsymbol{\eta}}_l, \tag{16}$$

where $\widetilde{\boldsymbol{\theta}}_l = [\widetilde{\boldsymbol{\theta}}_{l,0}^T, \ldots, \widetilde{\boldsymbol{\theta}}_{l,M-1}^T]^T$, $\widetilde{\boldsymbol{\Psi}}_l = [\widetilde{\boldsymbol{\Psi}}_{l,0}^T, \ldots, \widetilde{\boldsymbol{\Psi}}_{l,M-1}^T]^T$, and $\widetilde{\boldsymbol{\eta}}_l = [\widetilde{\boldsymbol{\eta}}_{l,0}^T, \ldots, \widetilde{\boldsymbol{\eta}}_{l,M-1}^T]^T$.

Because the vectors $\widetilde{\mathbf{s}}_l$ represent images of the same scene, a final composite image of the scene can be obtained by using image fusion techniques after each single-view image has been reconstructed and aligned [2, 22]. Here instead we propose to first combine the coefficient vectors from different views, then perform fusion using joint Bayesian sparse learning. Since the imaging coordinates are different between views, we need to adopt a pixel scanning scheme in which all the vectors $\widetilde{\mathbf{s}}_l$ have the same sparsity support [23]. Therefore, a linear imaging model relating a composite coefficient vector $\widetilde{\boldsymbol{\theta}}$ to the fused image of the scene $\widetilde{\mathbf{s}}$ can be formulated as a linear combination of the coefficient vectors of different views:

$$\widetilde{\boldsymbol{\theta}} = \sum_{l=1}^{L} w_l\,\widetilde{\boldsymbol{\theta}}_l = \widetilde{\boldsymbol{\Psi}}\,\widetilde{\mathbf{s}} + \widetilde{\boldsymbol{\eta}}, \tag{17}$$

where w_l's are positive weights ($\sum_{l=1}^{L} w_l = 1$) computed based on mutual information (MI) [11], $\widetilde{\boldsymbol{\Psi}} = \sum_{l=1}^{L} w_l\,\widetilde{\boldsymbol{\Psi}}_l$, and $\widetilde{\boldsymbol{\eta}} = \sum_{l=1}^{L} w_l\,\widetilde{\boldsymbol{\eta}}_l$. By combining this composite linear model with (16), we obtain an overall multitask model for the multi-view TWRI problem:

$$\widetilde{\boldsymbol{\theta}}_l = \widetilde{\boldsymbol{\Psi}}_l\,\widetilde{\mathbf{s}}_l + \widetilde{\boldsymbol{\eta}}_l,\ l = 1, \ldots, (L+1) \tag{18}$$

where $\widetilde{\boldsymbol{\theta}}_{L+1} = \widetilde{\boldsymbol{\theta}}$, $\widetilde{\boldsymbol{\Psi}}_{L+1} = \widetilde{\boldsymbol{\Psi}}$, $\widetilde{\mathbf{s}}_{L+1} = \widetilde{\mathbf{s}}$, and $\widetilde{\boldsymbol{\eta}}_{L+1} = \widetilde{\boldsymbol{\eta}}$. The solution of (18) yields $L+1$ images corresponding to the L individual views plus a composite image of the scene. This multitask problem can be solved efficiently using the joint Bayesian sparse model which exploits inter-view correlations.

4. EXPERIMENTAL RESULTS AND ANALYSIS

In this section, we present the experimental results obtained using simulated EM data. Experimental analysis and comparison with existing compressed TWRI models are also provided.

4.1. Experimental Setup

Electromagnetic (EM) simulations were performed to generate radar signals using XFDTD, a full-wave EM simulator. The scene behind a concrete wall containing two dihedral targets is illuminated from two different aspect angles: 0° view (from the front wall) and 90° view (through the side wall of the enclosed structure), see Fig. 1. At each view, the transceiver is placed at 51 positions parallel to the wall at a standoff distance of 1 m, to synthesize an array aperture of length 1.2 m. The transmitted frequency range is 1 GHz, centered at 2.5 GHz, with a step frequency of 3 MHz (i.e. 334 frequency bins). For sparsifying the signals, the dictionary $\mathbf{W}$ is constructed using Daubechies wavelet of order 4, with 3 decomposition levels.

The normalized mean squared error is used to measure the accuracy of the signal recovery:

$$\mathrm{NMSE} = ||\mathbf{z} - \hat{\mathbf{z}}||_2 / ||\mathbf{z}||_2, \tag{19}$$

where $\hat{\mathbf{z}}$ and $\mathbf{z}$ are the reconstructed and true signals, respectively. The image quality is measured using the target-to-clutter ratio (in dB):

$$\mathrm{TCR} = 10\log_{10}(P_{\mathrm{target}}/P_{\mathrm{clutter}}), \tag{20}$$

where P_{target} and P_{clutter} are the average power in the target and clutter regions, respectively. The receiver operating characteristic (ROC) curve is used to measure the probability of target detection for a given false alarm rate. The probability of detection, or detection rate, denotes the percentage of pixels in target regions that are correctly detected. By contrast, the probability of false alarm, or false alarm rate, is the percentage of pixels in the clutter region that are incorrectly detected as targets.

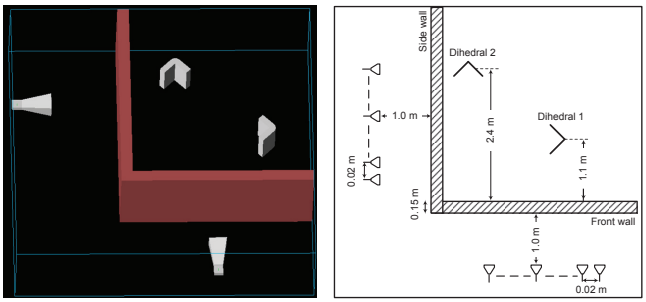

Fig. 1. Multi-view TWRI data acquisition for an enclosed structure target scene. Left: a photo of the scene; Right: a top-view of the behind-the-wall scene.

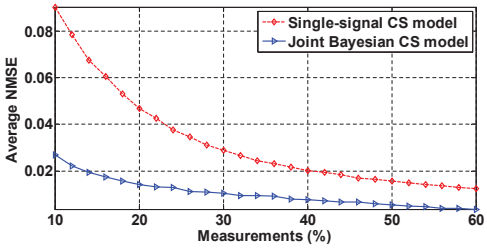

Fig. 2. The NMSE for signal reconstruction using the single-signal CS model and the joint Bayesian CS model.

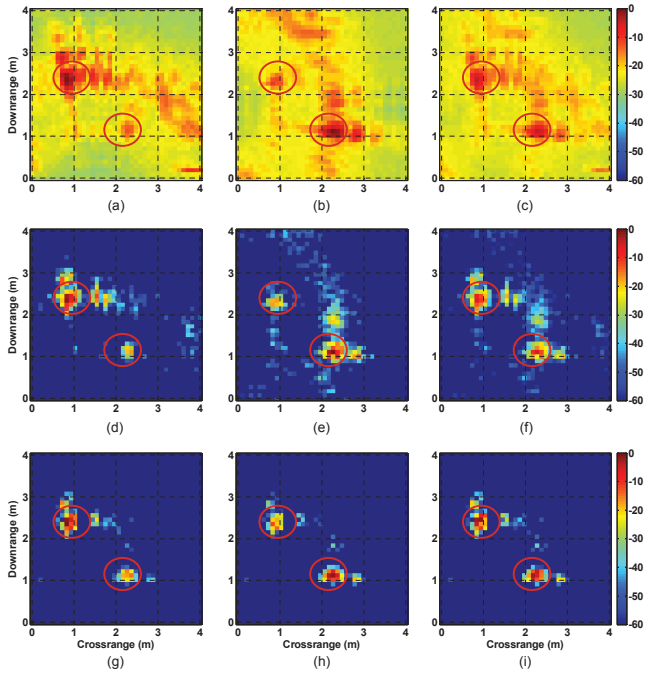

Fig. 3. The scene reconstructed by different approaches: (a) front wall image by DS, (b) side wall image by DS, (c) composite DS image; (d) front wall image by CS, (e) side wall image by CS, (f) composite CS image; (g)-(i) font wall, side wall, and composite images by the joint Bayesian sparse reconstruction.

4.2. Results and Analysis

In the first experiment, we used only 40% of the antennas and varied the number of frequencies from 10% to 60% at each view. For each set of measurements, the signals were recovered by the single-signal CS and joint Bayesian models; the NMSE was recorded for 50 trials. Figure 2 shows the average NMSE for both models. Compared to the separate CS model, the joint Bayesian model produces a considerably lower reconstruction error, especially when the measurements are drastically reduced. Moreover, to obtain the same reconstruction accuracy, the proposed approach requires far fewer measurements than does the single-signal CS model. For example, to obtain an NMSE = 0.027, the joint Bayesian sparse approach requires only 10% of the frequency measurements, whereas the single-signal CS model uses 30%. The superiority of the reconstruction by the joint Bayesian sparse signal model is due to the fact that this model exploits the signal sparsity and the correlations among the signals.

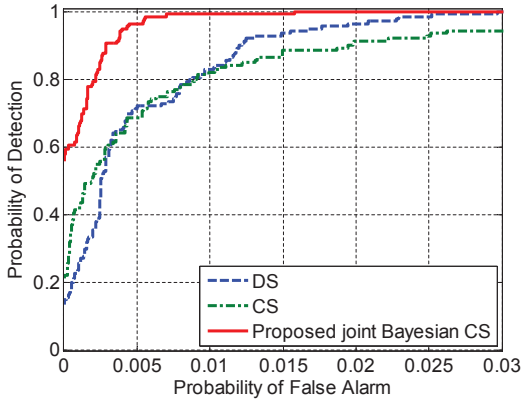

Fig. 4. ROC curves of the thresholding of composite images formed by different imaging approaches. See electronic color figure.

In the second experiment, the signals recovered with the joint Bayesian sparse model using 12% of the total measurements are used for scene reconstruction, after wall clutter mitigation. Figures 3(a)-(b) show the single-view images formed using DS beamforming; they contain sidelobes and heavy clutter. Furthermore, these single-view images do not provide a complete picture of the scene content because the signal returns of dihedral 1 are weak in the frontal view and the returns of dihedral 2 are weak in the side view. Figure 3(c) presents the image fused by MI-based method using these two DS formed images as input. This image still contains heavy clutter. Figures 3(d)-(f) present images obtained separately from the front view, side view, and their fused image, respectively, using the conventional CS reconstruction. We can observe the appearance of outliers in these images. By contrast, Figs. 3(g)-(i) show the images formed by the joint Bayesian sparse model, which contain much less clutter and reveal all the targets. The TCRs of the composite scene images formed by DS beamforming, the conventional CS, and the proposed Bayesian approach are 26.53 dB, 53.37 dB, and 75.45 dB, respectively. Figure 4 illustrates the ROC curves of the different imaging models. This figure shows that by jointly reconstructing multiple images target detection is significantly enhanced, compared with the methods that form the images individually at each view.

5. CONCLUSION

This paper presented a new approach for compressed multi-view TWRI using joint Bayesian sparse representation. In the proposed approach, a joint Bayesian sparse approximation is employed for estimating simultaneously the signal coefficients of different antennas from a reduced set of measurements. This joint Bayesian estimation exploits the sparsity and correlation among antenna signals. A subspace projection technique is applied directly to the recovered coefficients to segregate wall reflections from the target returns. Furthermore, a multitask imaging model is developed which combines the filtered coefficients for scene image formation. Individual images from each view and a composite image of the scene are reconstructed using joint Bayesian sparse learning, taking into account the inter-view dependencies. Experimental results show that the proposed approach enhances the scene image, compared with methods forming images separately for each view.

6. REFERENCES

[1] M. G. Amin (Ed.), *Through-The-Wall Radar Imaging*. Boca Raton, FL: CRC Press, 2010.

[2] C. H. Seng, A. Bouzerdoum, M. G. Amin, and S. L. Phung, "Probabilistic fuzzy image fusion approach for radar through wall sensing," *IEEE Trans. Image Processing*, vol. 22, no. 12, pp. 4938–4951, Dec. 2013.

[3] F. Ahmad and M. G. Amin, "Multi-location wideband synthetic aperture imaging for urban sensing applications," *Journal of the Franklin Institute*, vol. 345, no. 6, pp. 618–639, Sep. 2008.

[4] G. Wang and M. G. Amin, "Imaging through unknown walls using different standoff distances," *IEEE Trans. Signal Processing*, vol. 54, no. 10, pp. 4015–4025, Oct. 2006.

[5] C. Debes, M. G. Amin, and A. M. Zoubir, "Target detection in single- and multiple-view through-the-wall radar imaging," *IEEE Trans. Geoscience and Remote Sensing*, vol. 47, no. 5, pp. 1349–1361, May 2009.

[6] D. L. Donoho, "Compressed sensing," *IEEE Trans. Information Theory*, vol. 52, no. 4, pp. 1289–1306, Apr. 2006.

[7] E. J. Candes, J. Romberg, and T. Tao, "Stable signal recovery from incomplete and inaccurate measurements," *Communications on Pure and Applied Mathematics*, vol. 59, no. 8, pp. 1207–1223, Aug. 2006.

[8] Q. Huang, L. Qu, B. Wu, and G. Fang, "UWB through-wall imaging based on compressive sensing," *IEEE Trans. Geoscience and Remote Sensing*, vol. 48, no. 3, pp. 1408–1415, Mar. 2010.

[9] Y.-S. Yoon and M. G. Amin, "Through-the-wall radar imaging using compressive sensing along temporal frequency domain," in *Proc. IEEE Int. Conf. Acoustics, Speech, and Signal Processing*, Dallas, TX, Mar. 2010, pp. 2806–2809.

[10] V. H. Tang, A. Bouzerdoum, and S. L. Phung, "Two-stage through-the-wall radar image formation using compressive sensing," *Journal of Electronic Imaging*, vol. 22, no. 2, pp. 021 006–1–021 006–10, Apr.-Jun. 2013.

[11] A. Bouzerdoum, J. Yang, and F. H. C. Tivive, "Compressive sensing for multi-polarization through-the-wall radar imaging," in *Compressive Sensing for Urban Radar*. M. G. Amin (Ed.), Boca Raton, FL: CRC Press, Aug. 2014, pp. 232–248.

[12] E. Lagunas, M. G. Amin, F. Ahmad, and M. Najar, "Joint wall mitigation and compressive sensing for indoor image reconstruction," *IEEE Trans. Geoscience and Remote Sensing*, vol. 51, no. 2, pp. 891 – 906, Feb. 2013.

[13] V. H. Tang, A. Bouzerdoum, S. L. Phung, and F. H. C. Tivive, "Enhanced wall clutter mitigation for through-the-wall radar imaging using joint Bayesian sparse signal recovery," in *Proc. IEEE Int. Conf. Acoustics, Speech and Signal Processing*, Florence, Italy, May 2014, pp. 7804–7808.

[14] F. Ahmad, J. Qian, and M. G. Amin, "Wall clutter mitigation using discrete prolate spheroidal sequences for sparse reconstruction of indoor stationary scenes," *IEEE Trans. Geoscience and Remote Sensing*, vol. 53, no. 3, pp. 1549–1557, Mar. 2015.

[15] S. Ji, D. Dunson, and L. Carin, "Multitask compressive sensing," *IEEE Trans. Signal Processing*, vol. 57, no. 1, pp. 92–106, Jan. 2009.

[16] M. E. Tipping and A. C. Faul, "Fast marginal likelihood maximisation for sparse Bayesian models," in *Proc. the Ninth Inter. Workshop on Artificial Intelligence and Statistics*, Key West, FL, Jan. 2003, pp. 3–6.

[17] Q. Wu, Y. D. Zhang, M. G. Amin, and B. Himed, "Complex multitask Bayesian compressive sensing," in *Proc. IEEE Int. Conf. Acoustics, Speech and Signal Processing*, Florence, Italy, May 2014, pp. 3375–3379.

[18] Y.-S. Yoon and M. G. Amin, "Spatial filtering for wall-clutter mitigation in through-the-wall radar imaging," *IEEE Trans. Geoscience and Remote Sensing*, vol. 47, no. 9, pp. 3192–3208, Sep. 2009.

[19] F. H. C. Tivive, A. Bouzerdoum, and M. G. Amin, "An SVD-based approach for mitigating wall reflections in through-the-wall radar imaging," in *Proc. IEEE Radar Conf.*, Kansas City, MO, May 2011, pp. 519–524.

[20] F. H. C. Tivive and A. Bouzerdoum, "An improved SVD-based wall clutter mitigation method for through-the-wall radar imaging," in *Proc. IEEE Workshop on Signal Processing Advances in Wireless Communications*, Darmstadt, Germany, June 2013, pp. 430–434.

[21] F. H. C. Tivive, A. Bouzerdoum, and M. G. Amin, "A subspace projection approach for wall clutter mitigation in through-the-wall radar imaging," *IEEE Trans. Geoscience and Remote Sensing*, vol. 53, no. 4, pp. 2108–2122, Apr. 2015.

[22] C. H. Seng, A. Bouzerdoum, M. G. Amin, and S. L. Phung, "Two-stage fuzzy fusion with applications to through-the-wall radar imaging," *IEEE Geoscience and Remote Sensing Letters*, vol. 10, no. 4, pp. 687–691, July 2012.

[23] J. Yang, A. Bouzerdoum, and M. G. Amin, "Multi-view through-the-wall radar imaging using compressed sensing," in *Proc. European Signal Processing Conference*, Aalborg, Denmark, Aug. 2010, pp. 1429–1433.